#26

FERMILAB-CONF-76-113-E

NATIONAL ACCELERATOR LAB.
JUN 3 1976
PROGRAM PLANNING OFFICE

MSU-CSL-33
May, 1976

Dimuon and Trimuon Production in Deep Inelastic Muon Interactions at 150 GeV*

K. Wendell Chen
Michigan State University
East Lansing, Michigan
48823

Invited Talk Given at the

International Conference on New Particles
with New Quantum Numbers
University of Wisconsin, Madison, Wisconsin
April 21-23, 1976

---

*Work supported in part by the National Science Foundation under Grant No. GP29070

Abstract

Dimuon and trimuon events have been observed in deep inelastic muon interaction at 150 GeV. A preliminary analysis is presented. Taken at face value, the data suggest the existence of a new particle production mechanism. The rate of dimuon production occurs at 0.1% of inclusive deep inelastic muon scattering. High inelasticity trimuons occur at a rate one order of magnitude lower.

I. Introduction

I wish to first review data on two tests of scaling in muon scattering performed at Fermilab. These data have already been published previously.[1,2]

I will present new results on multimuon production by muons. The analysis of the data was carried out largely by myself in collaboration with Dr. C. Chang at Michigan State and with Dr.A. VanGinneken (Fermilab) whose contributions on π/K decay background calculations were invaluable. However any errors or inaccuracies contained in the data presented here are mine.

The multimuon events are unlikely from π/K's produced in deep inelastic muon interactions. Because of the somewhat limited statistics of our sample, qualitative conclusions are presented at this time. Further analysis on dimuon and trimuon data is now continuing. More data are expected in a Michigan State-Fermilab muon experiment currently in progress.

During the past year our views on scaling in deep-inelastic muon scattering changed somewhat. We now entertain the idea that as one reaches sufficiently high Q^2 and W^2, strict Bjorken scaling may not be valid. In the large ω region, the observed rates exceed the scaling predictions (using SLAC structure function at low energy) by about 20%. At low values of ω there is evidence for a depletion of events when the scaling variable ω' is used.[1,2]

The rise at large ω supports the idea of some new hadronic degrees of freedom, charm, color, or other exotic particle production. On the other hand, a combination of logarithmic behavior for the moments of structure functions and production mechanism at high Q^2 and W cannot be ruled out from the data at this time.

We have seen somewhat surprisingly, colliding beam measurements pointed to a rising e^+e^- total cross section, in contradiction with a simple parton model. In hadron-hadron interactions, Drell-Yan[3] production of massive e^+e^- pairs is still in a hazy state.[4] In neutrino scattering, observed energy dependence of the scaling variable $\langle Y \rangle$[5] indicates the breakdown of scaling. In short the validity of Bjorken scaling beyond the SLAC region is still very much in question.

More recently, we also witnessed the dramatic discoveries of J/ψ (and other particles) in e^+e^- annihilation and hadron-hadron collisions[6,7] as well as observation of dimuons in ν collisions[8]. The multimuon production data I present here should help to answer some questions regarding the origin of possible production mechanism in deep inelastic collisions.

II. Tests of Scaling in Muon Inclusive Scattering

Since any new production mechanisms may well be related to the validity of scaling in μp scattering, we first review general features of tests of scaling in μp scattering. The scaling tests are performed in two ways at Fermilab:

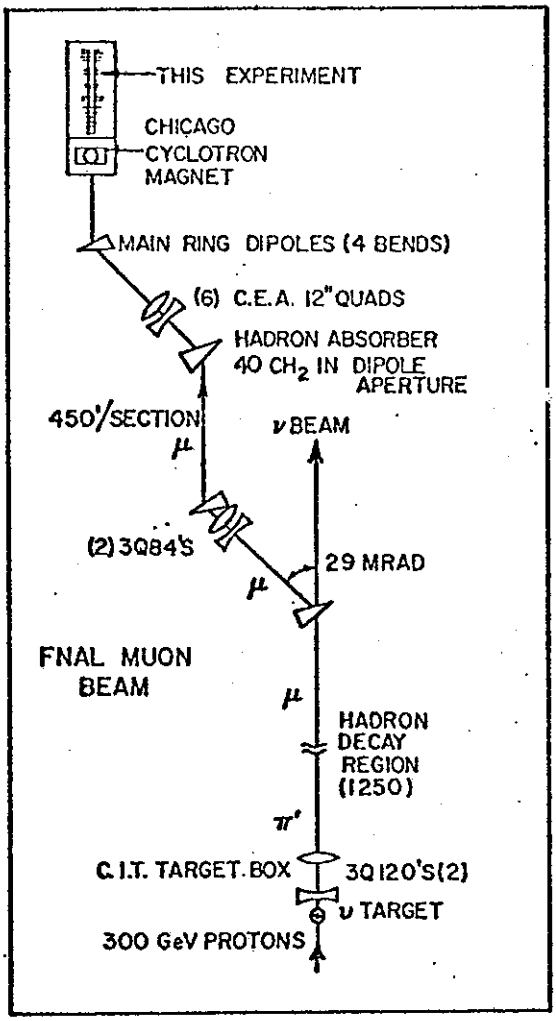

Fig. 1 150 GeV muon beam layout at Fermilab

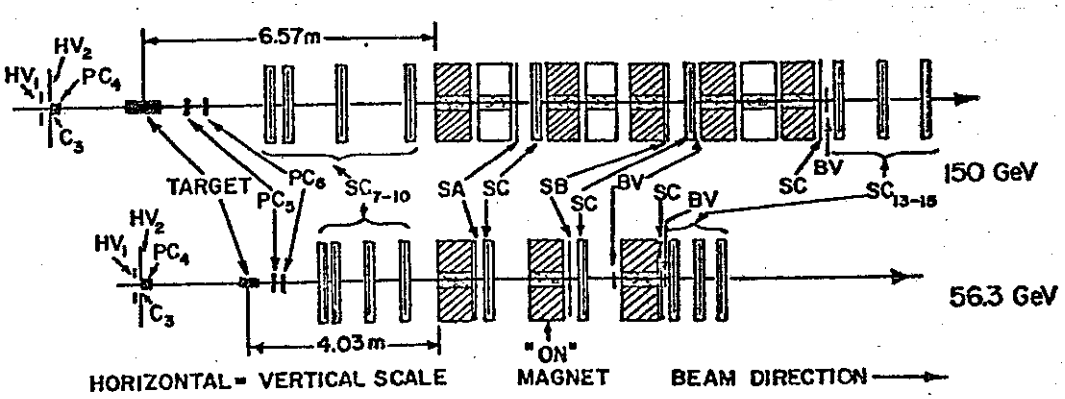

Fig. 2. Apparatus for muon scattering experiment at Fermilab.

a. Comparison of data at one energy and configuration with data at another energy and configuration.

b. Comparison with absolute predictions given by a Monte Carlo calculations assuming SLAC νW_2.

The apparatus was constructed to measure the direct ratio of scale-invariant differential cross sections at 150 and 56 GeV. The experimentally measured ratio, $\underline{r}(\omega, Q^2)$, defined by

$$\underline{r}(\omega, Q^2) = \frac{E\frac{d^2\sigma}{dxdy}\,(E=150)}{E\frac{d^2\sigma}{dxdy}\,(E=56)} \quad . \tag{1}$$

The experimental apparatus was scaled to change experimental quantities by $\lambda = 8/3$: $E_0 \to \lambda E_0$ (increase muon energy from 56 GeV to 150 GeV), $E' \to \lambda E'$ (increase total field integral by 8/3) and finally $\theta \to \frac{1}{\sqrt{\lambda}}\,\theta$ (scale target to spectrometer distance by $\frac{1}{\sqrt{\lambda}}$). See Figure 1 and 2.

As a direct result of these transformations, $Q^2 \to \lambda Q^2$ and $\nu \to \lambda\nu$, so that ω remains unchanged. Since $d^2\sigma/dxdy \to \frac{1}{\lambda}\,(d^2\sigma/dxdy)$, $\underline{r}(Q^2, \omega)$ is constant for all values of ω and Q^2, if Bjorken scaling were to hold in the high energy ($E_0 > 20$ GeV) region.

Figure 3 depicts $\underline{r}$ as a function of only ω.

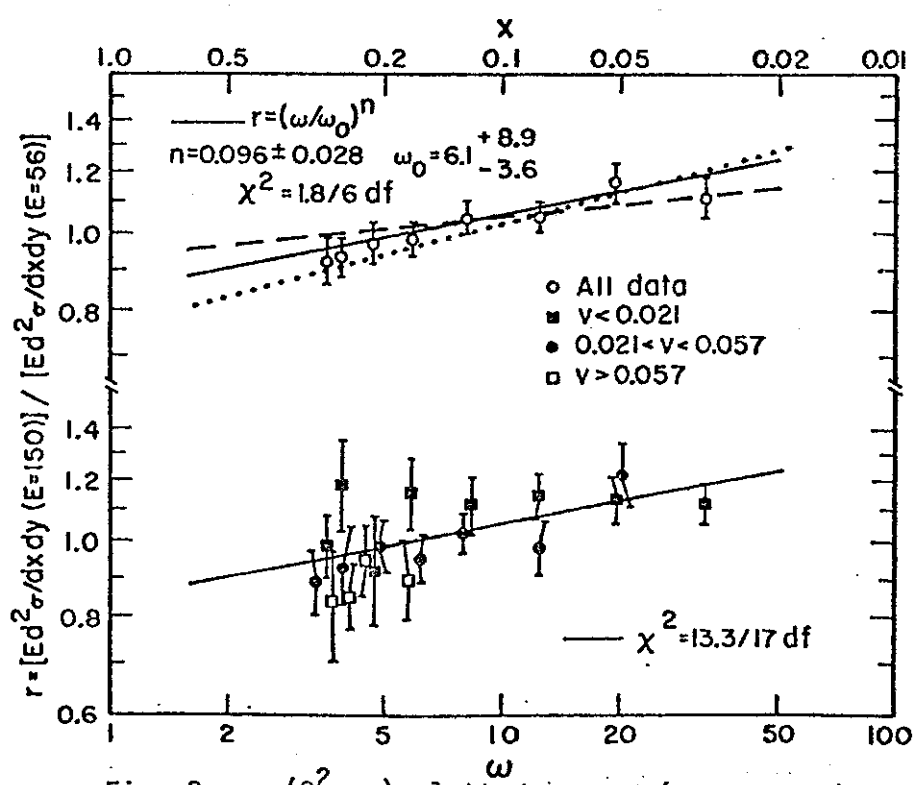

Fig. 3 $\underline{r}(Q^2,\omega)$ plotted vs ω (see Ref. 1)
v is defined as $Q^2/2ME$.

A statistically favorable hypothesis is that $\underline{r}$ depends only on ω. In this case the scale-breaking parameter $\underline{b} = \partial^2 \ln(\nu W_2)/\partial \ln(\omega') \, \partial \ln Q^2$ is nearly equal to the exponent of the power-law fit to $\underline{r}$ vs ω. If assumed to be ω independent, the parameter $\underline{b}$ is 0.098 ± 0.028. It should be emphasized that $\underline{b}$ is presented only as a guide to the systematic trend of the data. It is not necessarily a physically significant parameter in deep inelastic phenomena.

The second test of scaling compares these cross sections with lower-energy electron-scattering values assuming the validity of μ-e universality. Within fixed bands of ω, variations of νW_2 are evaluated over the full Q^2-range of the data. Thereby, with an accurate Monte-Carlo calculation of the experiment, a scaling test more precise than data/data method is possible.

Ratios of observed to Monte-Carlo event rates are shown in Fig. 4 vs $\ln Q^2$ for 8 overlapping bands of ω. The points show also a rising trend with Q^2 at high ω, and a falling trend at low ω. Fitting a power law Q^2-dependence in each band yields an overall χ^2 of 45.6 for 51 degrees of freedom. These 8 fitted slopes $\partial \ln(\nu W_2)/\partial \ln(Q^2)$ are plotted vs ω in the range of these data, the scale-breaking may be parameterized by a quantity $\underline{b} = \partial^2 \ln(\nu W_2)/\partial \ln(\omega') \partial \ln(Q^2)$. If independent of both Q^2 and ω, $\underline{b}$ has the

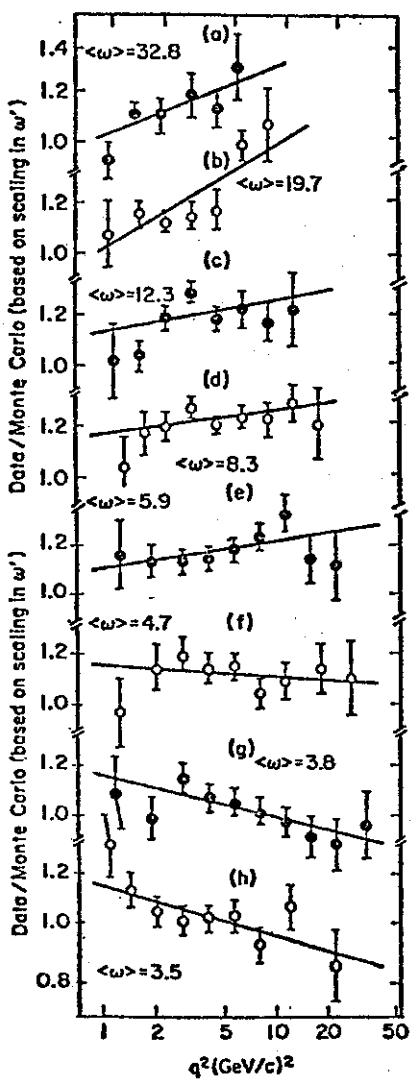

Fig. 4 Ratio of observed to Monte-Carlo rate vs Q^2 for 8 rangers of ω. Widths of these ranges and parameters of the straight-line fits are detailed in Reference 2. Errors are statistical. Note that $\langle W^2 \rangle \simeq Q^2 \cdot \omega$ in this figure.

magnitude (when fitted to $\ln\omega/\omega_0$), $\underline{b}$ = 0.099 ± 0.018, ω_0 = 6.1 (+3.9/-2.4).

The observed scale-noninvariance is insensitive to the assumed form of νW_2, because the data are analyzed within bands of ω. The Q^2-dependence of νW_2 for $\omega \leq 6$ is coupled to the assumed form of its approach to asymptotic behavior. Use of ω as a scaling variable increases the scale-noninvariance in this range (Figure 5) while use of $(\omega + 1.4/Q^2)$ largely cancels it. Conversely, the Q^2-dependence of νW_2 for $\omega \geq 6$ is inconsistent with scaling in any variable not wildly different from ω, since νW_2 is nearly independent of ω in this range. Variation of R between ∞ at $Q^2 = 1$ and 0 at $Q^2 = 5$ $(\mathrm{GeV/c})^2$ can account for only 1/4 of the scale-noninvariance at $\omega \simeq 25$.

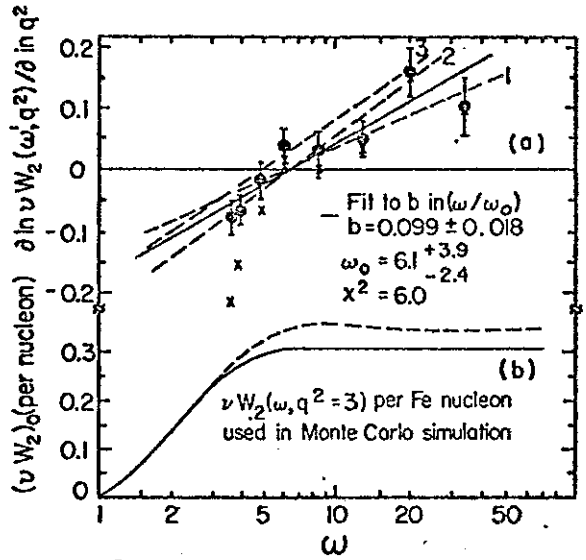

Fig. 5. (a) slopes in $\ln(Q^2)$ for the 8 ω ranges. Errors are statistical. Dashed lines depict effects of (1) raising E' by 1% at 150 GeV, (2) same at 56 GeV, (3) raising 150 GeV cross sections by 7%. Assuming scaling in ω rather than ω' in the Monte-Carlo yields the points indicated by "X".
(b) $\nu W_2(\omega, Q^2=3)$ per nucleon used in the Monte Carlo, with scaling in ω' and R=0.18. The dashed line is the alternate form described in the text.

In conclusion the empirical fit of our data is

$$\nu W_2(\omega', Q^2) = \nu W_2^{SLAC}(\omega') \left(\frac{\omega}{\omega_0}\right)^{b[\ln\frac{Q^2}{3}]} \qquad (2)$$

where

$$b = 0.099 \pm 0.018$$

$$\omega_0 = 6.1 \begin{smallmatrix} +3.9 \\ -2.4 \end{smallmatrix}$$

A qualitative behavior[9] of νW_2 is shown in Figure 6.

We have also examined the scale-breaking effects[10] using variables Q^2 and W. This is shown in Figure 7. For details concerning the curves show in the figure, one should consult Reference 10.

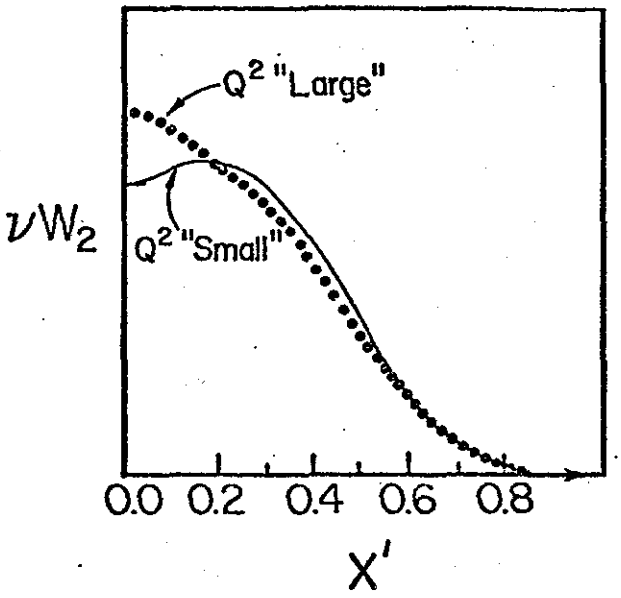

Fig. 6 Crude behavior of νW_2 (ω') at high Q^2.

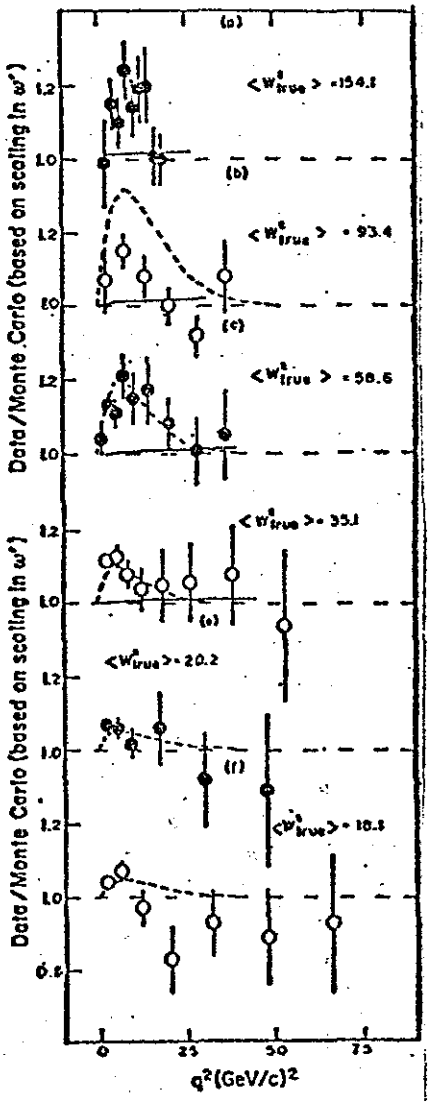

Figure 7 Data/Monte Carlo (assuming scaling in ω') vs Q^2 for six W^2 bins. (see Ref. 10)

III. Dimuon Events

1. We now discuss data events containing an extra muon in the final state in addition to the scattered muon. This search was motivated by the apparent excess of events at large ω. In Figure 8 we show the residue W distribution of events after subtraction from the number predicted using the SLAC (scaling) structure function. The distribution shows a provocative if not conclusive evidence in favor of a threshold effect. The solid curve is drawn to guide the eye. It should be noted that the distribution shown here is quite sensitive to the normalization of the data and apparatus acceptance at small value of ν.

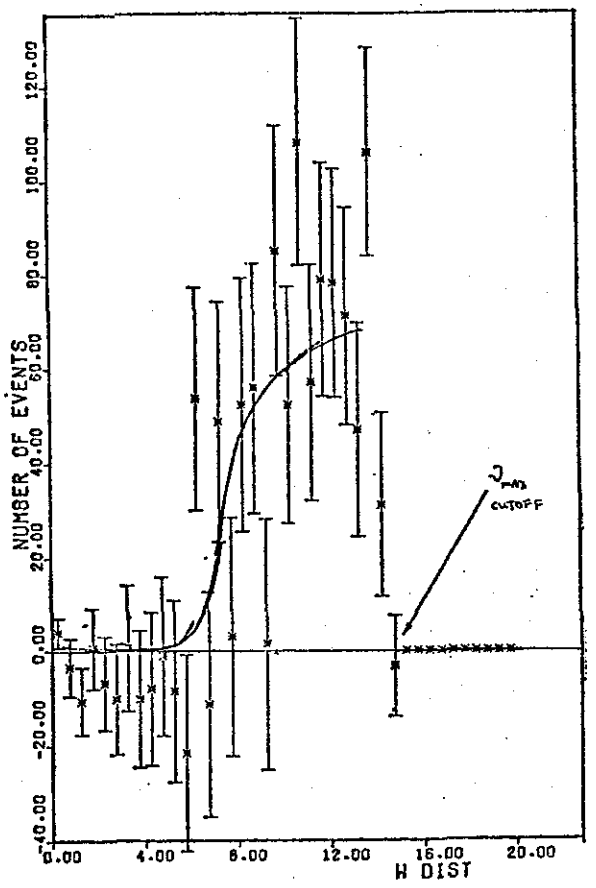

Figure 8. Number of events after subtraction from the number predicted using SLAC structure function is plotted vs W. The maximum W is limited by ν_{max} $(=E-E'_{Min})$. Note that this distribution is very sensitive to the normalization of the data.

Characteristics of 38 multimuon events are presented. Taken at face value, the data imply the existence of a new particle production mechanism in muon scattering.

The processes giving rise to an extra muon in the final state

$$\mu^+ + N \rightarrow \mu^+ + \mu^- + \text{hadrons} \qquad (1)$$
$$\rightarrow \mu^+ + \mu^+ + \text{hadrons}$$

$$\mu^- + N \rightarrow \mu^- + \mu^+ + \text{hadrons} \qquad (2)$$
$$\rightarrow \mu^- + \mu^- + \text{hadrons}$$

have been observed at the rate about 10^{-3} per deep inelastic muon scattering event ($E' > 17$ GeV and $\theta > 13$ mrad.).

Eleven events with three muons in the final state,

$$\mu^+ + N \rightarrow \mu^+ + \mu^+ + \mu^- + \text{hadrons} \quad (3)$$

$$\mu^- + N \rightarrow \mu^- + \mu^- + \mu^+ + \text{hadrons} \quad (4)$$

have also been observed at the rate exceeding 10^{-4} per deep inelastic muon scattering event defined above.

The muon beam was derived from a simple quadrupole triplet trainload tuned for 150 GeV charged hadrons. The primary proton energy for this experiment was 300 GeV. The trigger requirement for all multimuon events was a single scattered (or produced) muon penetrating the entire apparatus with an energy $E_\mu' > 17$ GeV. Single μ triggers are desirable as it introduced no biases in searching for the extra muon candidates. The apparatus is the same as the one used to study the validity of scaling. The apparatus has a region of zero magnetic field ($r < 6''$) about the beam axis. Two 12" diameter beam veto counters reject any charged particles that enter an inactive region defined by the third toroid magnet. The geometry of the apparatus is such that the extra muon can enter the region prior to the veto counters and be momemtum analyzed. We have found that substantial number of multimuon events are triggered by the produced muon at sufficiently large angles (~60%), rather by the scattered muon. This distinction is important since events triggered by the scattered muon should be used to determine the $\sigma(\mu \rightarrow \mu\mu)/\sigma(\mu \rightarrow \mu)$ rate in order to avoid complications caused by uncertainty associated with the acceptance for the produced muon. We note that inclusion of multimuon events which are triggered by the produced muon introduces a sizable distortion in the kinematical distributions presented here. Nevertheless, the statistics of our sample is still somewhat limited to warrant a careful segregation at this time except for branching ratio calculations. Although event finding program would have imposed a cut at $E_\mu' > 17$ GeV, multiple scattering made the cut at $\sim$12 GeV. Multimuon events were searched for in data runs with both μ^+ and μ^- beams to permit a study of the charge asymmetry of production process.

A candidate is considered an event by the scanning and measuring criteria:

1) Triggering muon (not necessarily the leading muon) must penetrate all magnets and well behaved traversing through the field region.

2) All muon trajectories (scattered and produced muons) must extrapolate to the beam line to within $\Delta \leq 2$ cm.

3) Triggering muon (not necessarily the leading muon) and the accompanying muon(s) can be momentum analyzed by at least one magnet.

4) Observed correct timing and hodoscope information for all final state muons.

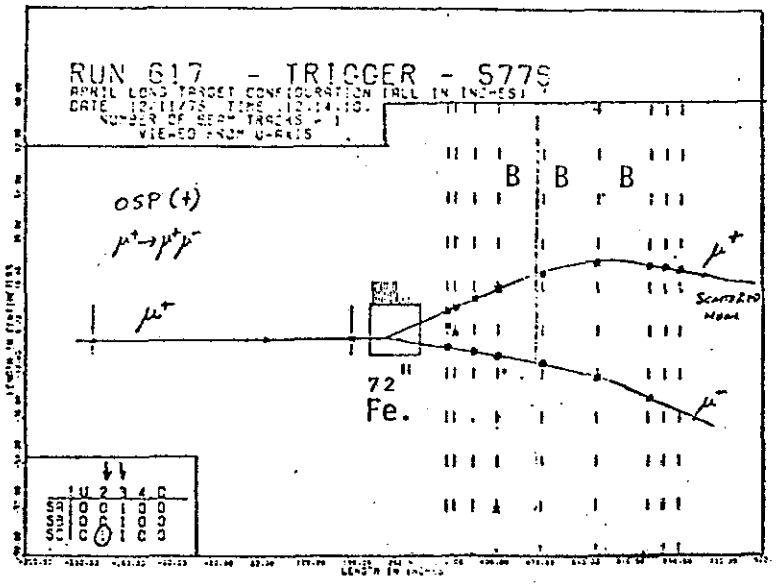

Figure 9. Typical dimuon event $\mu N \to \mu\mu X$. The target is 72" iron in length. The vertical lines above the target represents the cascade shower that accompany the interaction. The chambers cover an area 72" x 72". The areas indicated by "B" are regions of magnetic field.defined by the three toroidal magnets shown in Figure 2. A 6"-radius veto counter is located at the third magnet to reject small angle (thus low P_T) events and noninteracting beam muons.

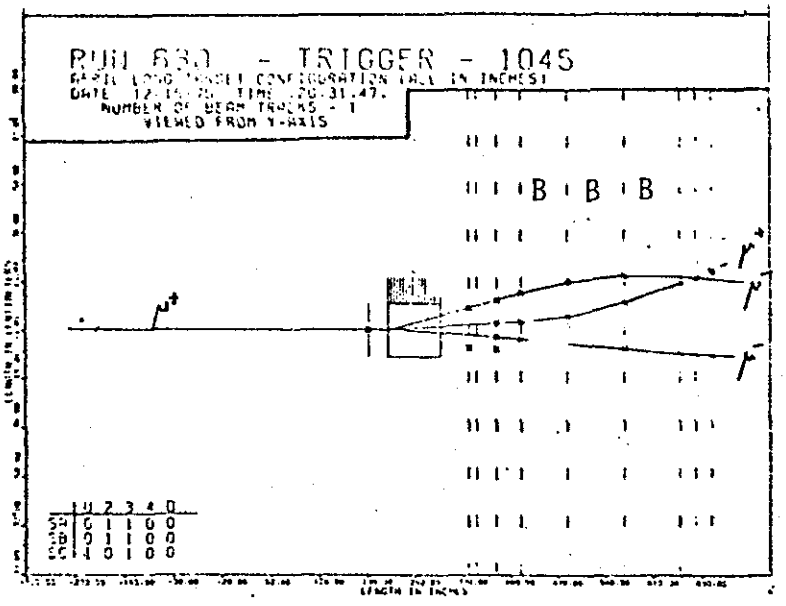

Figure 10. Typical trimuon event $\mu N \to \mu\mu\mu X$.

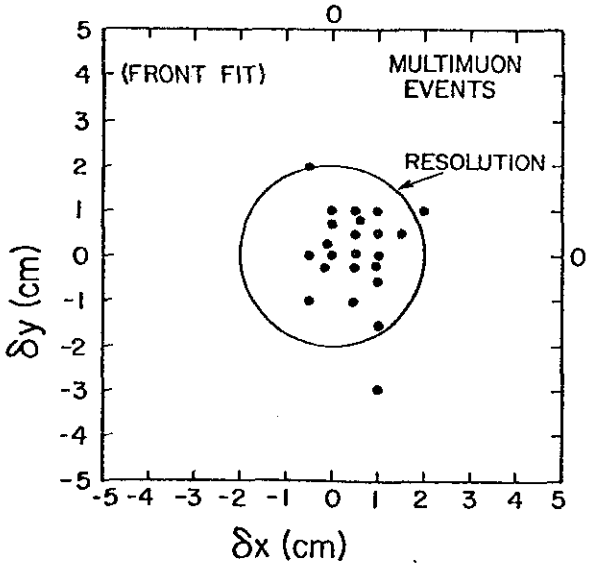

Figure 11. Extrapolated vertex position from muon beam axis. The resolution of measurement is shown in circle.

In this exposure, 8.8×10^9 muons were allowed to traverse a 72" Fe target at 150 GeV. The following table summarizes the result of the event finding analysis:

Total accepted single muon events (with E' > 17)	25,560
Good pairs found after scanning and measurement (See Table I)	27
Good trimuons found after scanning and measurement (See Table II)	11*

*(three 3μ events have ambiguity in one of the muon momenta)

2. Charge Asymmetry in Multimuon Production

$\mu^-\mu^+$, $\mu^+\mu^-$, $\mu^+\mu^+$, $\mu^-\mu^-$ and μμ μ events found are classified as "opposite-sign-pairs" (OSP), "same-sign-pairs" (SSP), and "trimuons" (TM), respectively as shown below. The first muon denotes the scattered muon.

	μ^+ Incident	Number of Events
OSP	$\mu^+ \to \mu^+\mu^-$	10
SSP	$\mu^+ \to \mu^+\mu^+$	5
TM	$\mu^+ \to \mu^+\mu^+\mu^-$	4
	$\mu^+ \to \mu^+\mu^+\mu^+$, $\mu^+\mu^-\mu^-$ (wrong sign)	0
	μ^- Incident	Number of Events
OSP	$\mu^- \to \mu^+\mu^-$	5
SSP	$\mu^- \to \mu^-\mu^-$	7
TM	$\mu^- \to \mu^-\mu^-\mu^+$	7
	$\mu^- \to \mu^-\mu^-\mu^-$, $\mu^-\mu^+\mu^+$ (wrong sign)	0

The charge asymmetry, A, after combining both μ^+ and μ^- data, is consistent with unity.

$$A_2 = \frac{\text{No. of same sign pairs}}{\text{No. of opposite sign pairs}} = \frac{12}{15} = 0.80 \pm 0.38$$

For 3μ events the fraction of wrong signature events to correct sign events, f, is

$$f = \frac{\text{No. of wrong sign TM's}}{\text{No. of correct sign TM's}} = \frac{0}{11} = 0.0 \pm 0.1$$

Within statistics, no charge asymmetry in 2μ events is observed. For 3μ events we observed no wrong-sign events.

3. Energy Distribution of Extra Muons (2μ)

Opposite-sign dimuons (OSP) can be used to study the leading particle effect. Since the charge of the scattered muon can be uniquely determined, we can measure the energy distributions of the produced muon, p_2 (p_1 is the scattered muon momentum). Figure 12 shows that p_1 p_2, suggesting a leading particle effect. This feature helps us to identify p_1 and p_2 in SSP 2μ events, in which both muons have the same sign. We find $\langle p_1\rangle/\langle p_2\rangle = 2.77$.

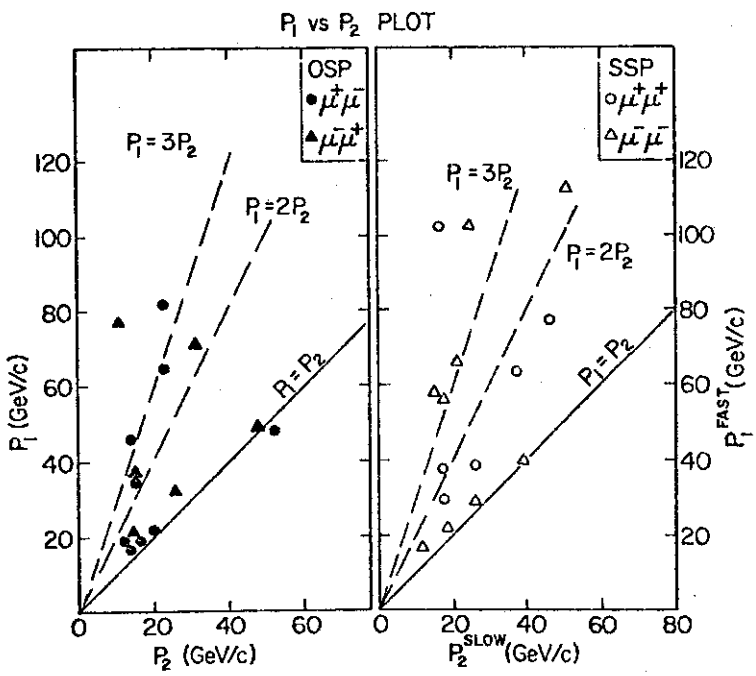

Figure 12. P_1 vs P_2 for OSP's and SSP's. For OSP's, P_1 is the muon having the same sign as the incoming muon. For SSP's, P_1 denotes the "fast" muon.

4. Q^2, X, W and $M_{\mu\mu}$ (2μ)

Figure 13 shows the Q^2 distribution for the OSP's. Figure 14 shows x distribution for 15 OSP's. We note that the average is $\langle x\rangle=0.05$. It is emphasized here that this is in the same region where some scaling violations are found.

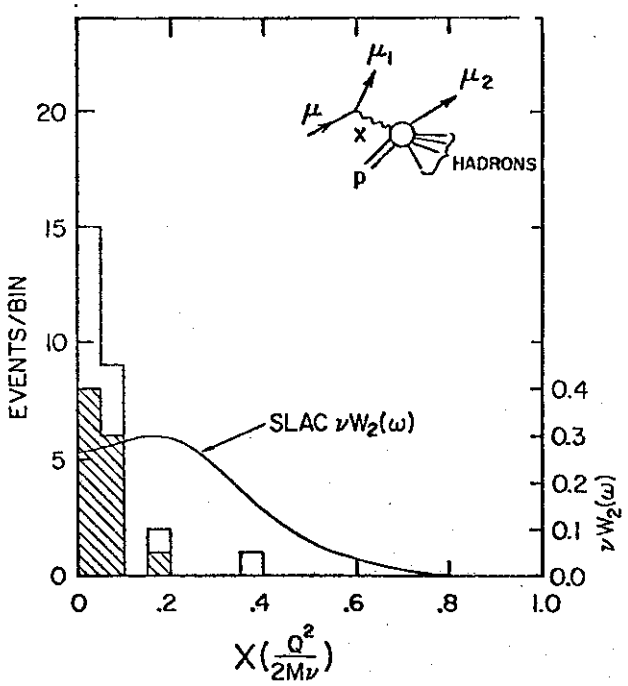

Figure 14. x distribution for OSP's.

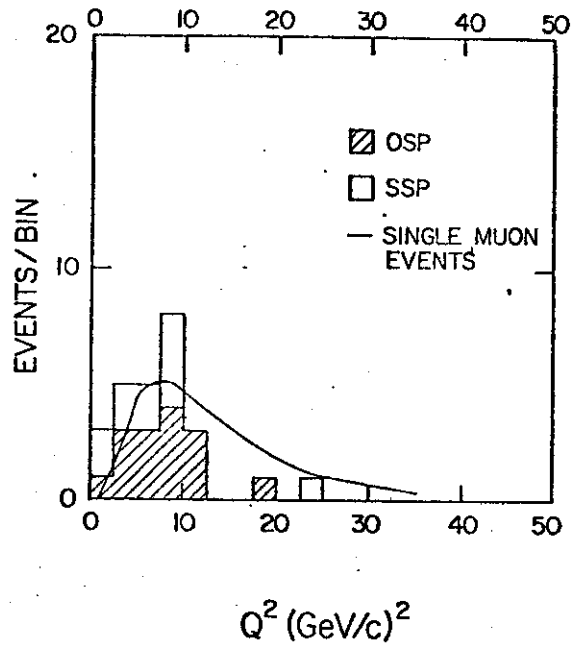

Figure 13. Q^2 distribution for OSP's are not plotted since the finite state muon have same sign.

The energy transfer to the virtual photon-nucleon system, $Y = \nu/E$, is shown in Figure 15. We observe a threshold at $Y = 0.3$. To better understand the 2μ sample, we plotted W vs Q^2 in Figure 16. We observe an apparent lower threshold at $W \approx 8$-9 GeV. The upper cut-off in the W distribution is dictated by the maximum energy transfer $\nu_{max} = 140$ GeV. The W distribution for single events is also shown in Figure 16.

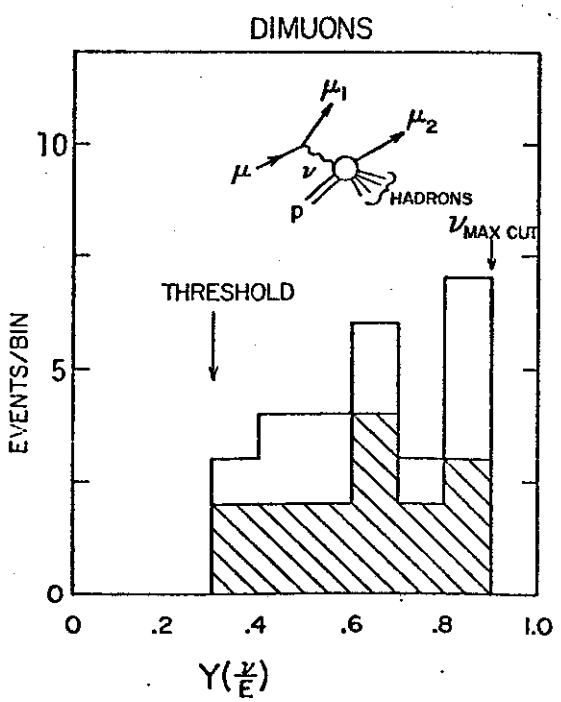

Figure 15. $y(\frac{\nu}{E})$ distributions for all pairs. The shaded areas are for OSP's and open areas are for SSP's.

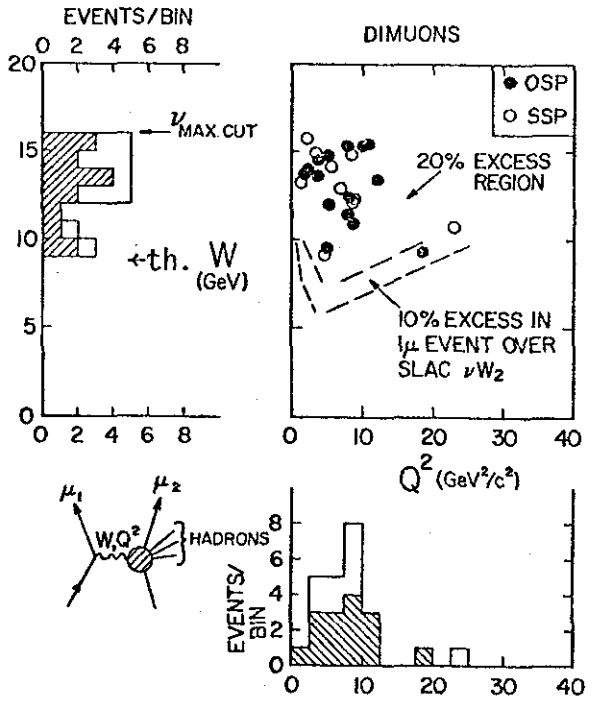

Figure 16. W vs Q^2 for all 2μ events. The projected distributions are shown.

If the muon pairs are direct decays of a massive object, then $M^2_{\mu\mu} = (p_1 + p_2)^2$, the invariant mass squared should show a peak. This is not seen in Figure 17. The mass resolution is estimated to be 20%.

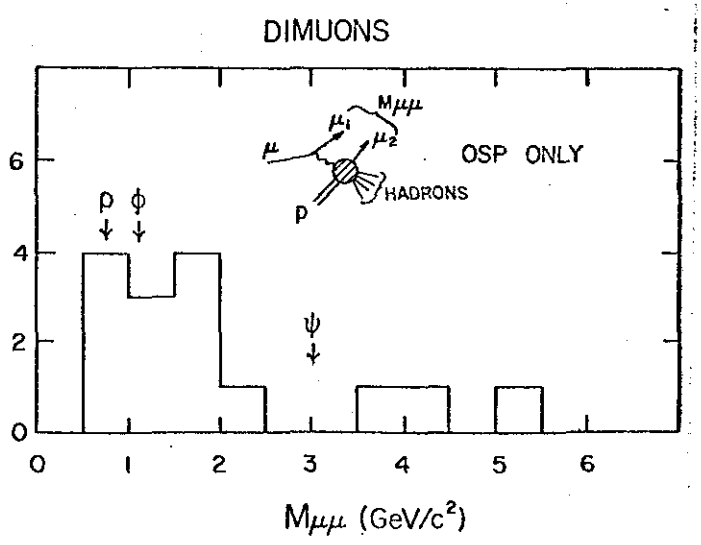

Figure 17. Apparent mass distribution between two opposite sign muons in OSP's. No peaks are seen.

5. P_T of the Extra Muon

In muon scattering, the virtual photon defines the direction from which transverse momenta of produced muons are measured. In ν scattering, on the other hand, a lack of information on the incident energy often prevents a good measure of direction of the hadron jet.

Figure 18 shows the uncorrected $(P_T)_2$ measured from the virtual photon direction vs E_2 for 27 dimuons.

For decays of π's or K's, one expects a distribution e^{-6P_T} around the direction of virtual photon. The observed P_T distribution is considerably flatter. The acceptance at low P_T region is suppressed due to the finite size muon beam, inner aperture of the toroidal magnets, and the inner opening of the trigger hodoscopes. For events with $P_T < 0.5$ GeV/c, the acceptance is estimated to be $\lesssim 10\%$. Since the acceptance is dependent on the production mechanism, work is needed to obtain a corrected spectrum. We note, however, that this suppression at low P_T conveniently reduces possible π/K decay backgrounds since $P_T(\pi \to \mu\nu)$ is ≤ 0.35 GeV/c.

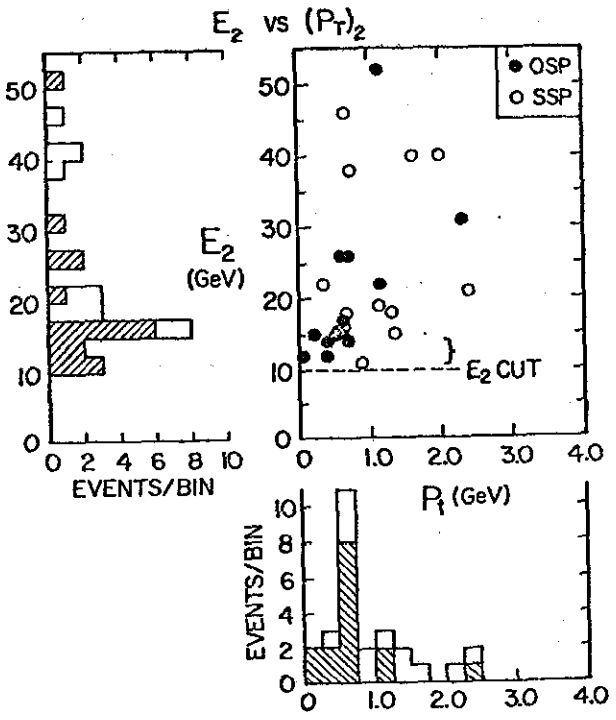

Figure 18. Energy of the extra muon. The E_2 cut is determined by the requirement that all muon to traverse through the entire toriodal magnets. $(P_T)_2$ is measured from the virtual photon direction. The effective cut on E_2 is $\sim$ 12 GeV.

6. Angular Distributions for $\Theta_{\mu\mu}$ and $\Delta\phi$.

The opening angle between dimuons is of interest since it permits an estimate of possible contaminations due to purely electromagnetic processes. For QED tridents, for example, $\Theta_{\mu\mu}$ should peak at small angles. This is not favored since, as shown in Figure 19, $\langle\Theta\rangle$ is 83 mrad. The apparent difference in the $\Theta_{\mu\mu}$ distribution between OSP's and SSP is due to focussing (defocussing) properties of the muon spectrometer for μ^+ and μ^-.

The azimuthal angles between the dimuons, $\Delta\phi_{12}$, are shown in Figure 20. No coplaner events are found, suggesting that dimuon events are not due to 2-body decays of resonant particles.

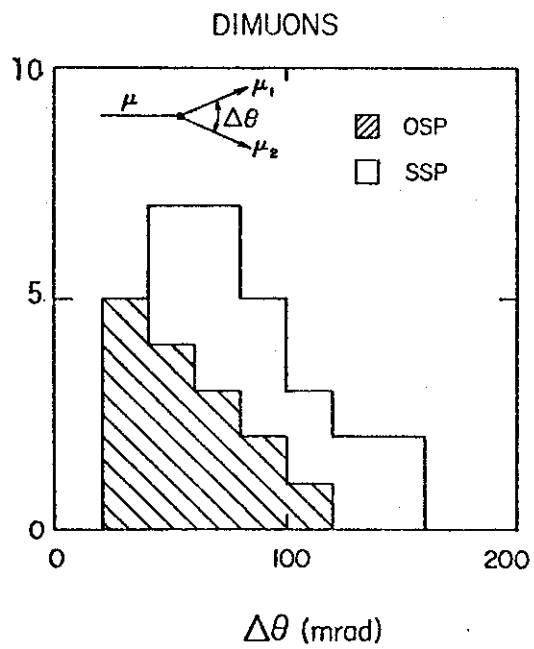

Figure 19. Opening angle distributions between dimuons in the final state. The apparent shift is due to the opposite sign of one of the dimuons (see text).

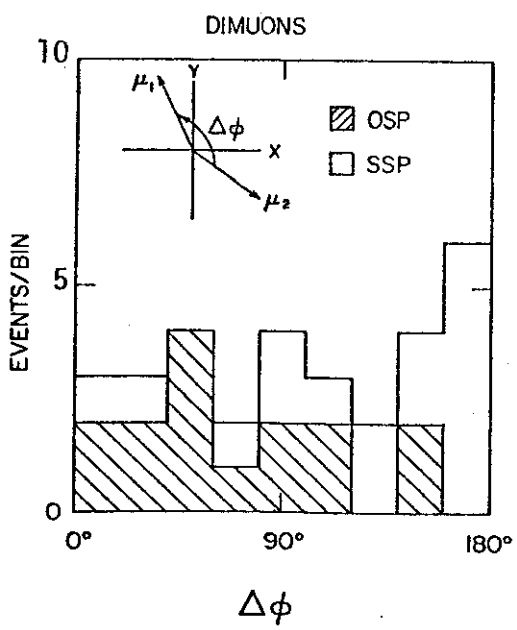

Figure 20. Azimuthal angle distributions between dimuons in the final state.

7. Summary of Dimuon Characteristics

The main features of our dimuon events prior to efficiency or acceptance corrections are:

i) Leading particle effects for opposite sign pairs, i.e. $p_1 > p_2$.

ii) No measureable charge asymmetry between OSP's and SSP's.

iii) Apparent cutoff of 9 GeV in the missing mass W.

iv) "Flat" P_T distribution up to 2.4 GeV/c ($\frac{dN}{dP_T} \sim e^{-1.8P_T}$).

v) No visible peak in apparent $M_{\mu\mu}$ mass.

vi) Generally large Q^2 and large ω ($\omega>10$) and $x \leq 0.10$. This region of x coincides with where excess events were found in single muon x distributions.

vii) High visible hadron inelasticity.

viii) No anomaly in $\Theta_{\mu\mu}$ and $\Delta\phi$ distributions.

TABLE I DIMUON EVENTS

$\mu^+\mu^-$

Event	E_1	E_2	$M_{\mu\mu}$	x	y	q^2	W	P_t	L_s (μ10cm)
1*	+46	-14	0.90	0.01	0.69	2.6	13.9	0.41	(≥4)
2	+82	-22	2.43	0.07	0.45	8.8	10.9	1.16	5
3	+94	-26	3.84	0.18	0.37	18.5	9.3	0.71	11
4	+35	-15	0.52	0.02	0.77	3.7	14.5	0.63	7
5*	+48	-52	4.05	0.07	0.68	12.3	13.4	1.14	(≥2)
6*	+18	-15	1.30	0.05	0.88	11.1	15.4	0.22	9
7*	+19	-13	1.50	0.04	0.87	9.9	15.3	0.55	(≥9)
8*	+99	-12	1.63	0.05	0.34	4.9	9.5	0.41	7
9	+50	-12	0.91	0.02	0.67	3.8	13.6	0.05	6
10	+63	-15	1.90	0.05	0.59	8.3	12.4	0.52	(≥2)

$\mu^+\mu^+$

Event	E_1	E_2	$M_{\mu\mu}$	x	y	q^2	W	P_t	L_s
1*	+64	+38	—	0.06	0.57	9.0	12.3	0.75	7
2*	+30	+18	—	0.02	0.80	3.5	14.9	1.31	9
3	+28	+22	—	0.04	0.81	8.4	14.8	0.35	10
4*	+76	+40	—	0.17	0.49	22.9	10.7	2.00	(≥2)
5*	+76	+46	—	0.36	0.49	49.5	9.4	0.67	3

$\mu^-\mu^+$

Event	E_1	E_2	$M_{\mu\mu}$	x	y	q^2	W	P_t	L_s (μ10cm)
1	-77	+17	1.05	0.06	0.49	7.9	11.4	0.62	0
2	-49	+14	1.20	0.01	0.67	1.9	13.7	0.69	6
3	-32	+26	1.52	0.02	0.79	5.3	14.7	0.60	4
4*	-20	+15	0.57	0.03	0.87	8.1	15.3	0.62	(≥6)
5	-71	+31	5.40	0.04	0.53	5.4	12.0	2.32	10

$\mu^-\mu^-$

Event	E_1	E_2	$M_{\mu\mu}$	x	y	q^2	W	P_t	L_s
1	-40	-40	—	0.03	0.73	5.8	14.1	1.62	4
2	-56	-18	—	0.01	0.63	1.5	13.2	0.68	5
3*	-57	-16	—	0.04	0.62	7.0	12.9	0.66	4
4*	-21	-19	—	0.03	0.86	8.0	15.3	1.12	10
5	-18	-11	—	0.01	0.88	2.3	15.7	0.87	4
6	-103	-15	—	0.06	0.31	4.7	9.1	1.36	(≥4)
7	-67	-21	—	0.06	0.55	8.7	12.1	2.41	7

* the leading particle triggered

+ Length of observed showers in units of 4" Fe.

IV. Backgrounds

We shall first discuss the background due to π/K decays and simulated μ trident events. In a later section other and more interesting origins will be discussed.

1. Pion and Kaon Decays

One of the most uninteresting origins of the observed extra muons is the decays of pions and kaons produced in deep inelastic collisions. Generally speaking π/K decays are characterized by:

1) low $(P_T)_2$ and E_2 owing to low mass of π and K's. Since our apparatus has low acceptances at low values of $(P_T)_2$ and P_2, most of π and K decays are already rejected.

2) no charge asymmetry in the π/K decays since both positive and negative particles are produced.

To estimate the level of 2μ and 3μ backgrounds from π/K decays, we used the measured pion production[11] cross sections at 150 Gev:

$$\frac{d^2\sigma}{dx'_F dp_T^2} = k \exp(-3.25x') \exp\{-b(P_T^2 + M^2)^{\frac{1}{2}}\}, \quad 0<x'<1 \qquad (5)$$

and

$$\frac{d^2\sigma}{dx'_F dp_T^2} = k \exp(-6.0x') \exp\{-b(P_T^2 + M^2)^{\frac{1}{2}}\}, \quad -1<x'<0 \qquad (6)$$

Other values of b ($\simeq$6) and M ($\simeq$0.8) have been tried. The π/K background is not sensitive to the choice around the measured values.

The observed hadron multiplicity in electro-production of pions is assumed to be

$$\langle n\rangle = 0.18 + 0.75 \log S - 0.075 \log Q^2, \quad (Q^2>1). \qquad (7)$$

For kaon production we assume $\frac{K}{\pi} = 0.1$. In calculating the muon yields from π and K-decay we allowed the incoming muon to interact uniformly in the 72" Fe target and π/K produced in the primary collision in turn interact making more (at lower hadron energy) secondary hadrons. This cascade process continues until the full shower is propagated through the entire target-toroid magnet detection system. The total integrated spectrum thus takes fully into account the development of hadron cascade and includes decay processes throughout the apparatus. We summarize the results of the π/K calculation in Figure 21, along with the observed integrated E_2 spectrum for 2 μ events.

The transverse momentum distribution of π/K decays is shown in Figure 22. We are able to account for events with $(P_T)_2<0.5$ (GeV/c) as due

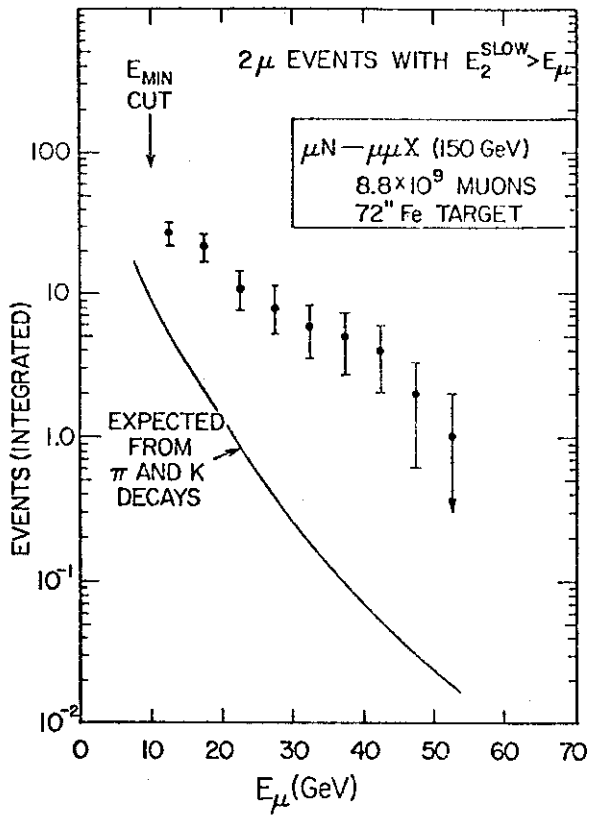

Figure 21. The dimuon events with extra muon energy $E_2 > E_\mu$ in muon interactions. Expected number of μ's arising from π or K-decay in hadron cascade is shown in solid curve. The low energy cut is due to the requirement that all muons must penetrate the entire spectrometer.

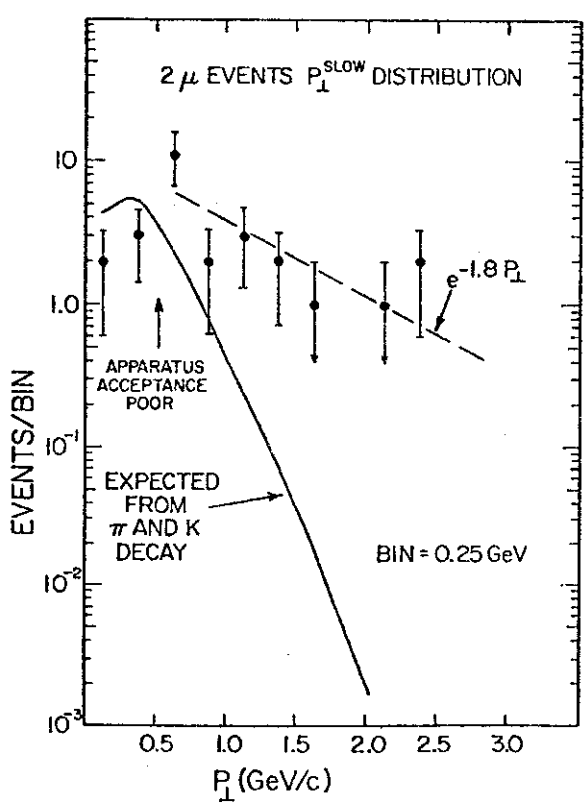

Figure 22. Transverse momentum distributions for the extra muon in the dimuon sample. The distribution expected from π and K-decays are shown in solid curve.

to π/K decays. The maximum level of contamination from π/K decays is estimated to be <20% of the entire 2 μ sample, prior to $a(P_T)_2$ cut.

2. QED Backgrounds in Dimuon Sample

We examined in some detail the kinematical properties of QED tridents. If one of the muons in a QED trident should have an energy less than a few GeV, the event may fake a dimuon event when the low energy muon stops in the target. Tridents with muons emitted in the forward direction will be vetoed if $\Theta_\mu < \Theta_{cut}$ (6 mrad) defined by the beam veto counter.

Monte Carlo trident events were generated according to the Bethe-Heither trident cross section defined by Brodsky and Ting[12], for 150 GeV muons on an iron target. The elastic form factor for an iron nucleus was taken as

$$\exp\left(-\frac{b^2}{6}Q^2\right) \;/\; \left(1+\frac{c^2}{6}Q^2\right) , \qquad (8)$$

where b = 24 fm. c = 1.07 x $A^{1/3}$fm. Events with a muon of E > 5 GeV and $\Theta_\mu < \Theta_{cut}$ were rejected. Muons with E < 10 GeV were considered undetected. The probability that this could happen as a function of Θ_{cut} is shown in the following.

Θ_{cut} (mr)	Probability (%) ($\pm$ 3%)
1	6.2
2	7.7
3	3.6
4	3.4

Our studies show that less than 3% of all tridents will have a low energy muon stoppable by the target or by other parts of the apparatus. The remaining 97% of tridents are detected with reasonable efficiency. This endorses our belief that the dimuon sample cannot all be of QED in origin unless the ratio of detection efficiencies for tridents is only 1.4% of that for dimuons. This is highly unlikely as extra muon detection efficiency is of the order 50% or more based on Monte-Carlo calculations.

We have not investigated in sufficient detail contributions from inelastic QED trident events. However, much of the same argument still applies here. Finally, a possibility exists that the third muon of a trident event may enter the "dead" region in the center of the muon spectrometer. Since beam veto counters (12" in radius) were included in our trigger, events of this kind would have been vetoed with high efficiency. In addition, the spark chamber would also have observed much of the third muon tracks should the muon escape detection caused by inefficiencies of the veto counters.

Genuine dimuon event losses caused by the beam veto counter can be crudely estimated by examining the opening angle distribution of the observed dimuons. $\langle\Theta_{\mu\mu}\rangle$ is $\sim$ 85 mrad. We estimated a maximum loss event of 20%.

V. Trimuons

The observation of 11 trimuon events (Table II) may well be of some significance. The information content in each of these events is quite large due to the large number of final state muons. The interpretation of these events is also necessarily more complex than 2 μ events.

First of all, no events of the type ($\mu_{leading}\ \mu^+\mu^+$) or ($\mu_{leading}\ \mu^-\mu^-$) have been observed out of 11 events. This is a strong experimental evidence against the prospect that extra muons are results of large multiplicity events in which many like-charge ordinary hadrons are produced and decay subsequently.

1. Inelasticity parameter, η,

For multimuon event, we define a inelasticity parameter, η, by

$$\eta_{2\mu} = \frac{E_0 - E_1 - E_2}{E_0} \quad \text{for } 2\mu \text{ events}$$

$$\eta_{3\mu} = \frac{E_0 - E_1 - E_2 - E_3}{E_0} \quad \text{for } 3\mu \text{ events}$$

The inelasticity distribution $\frac{dN}{d\eta}$ for 3μ's are shown in Figure 23a. This is to be compared with inelasticity distributions for 2μ's. (Fig.23b.) The distributions are different.

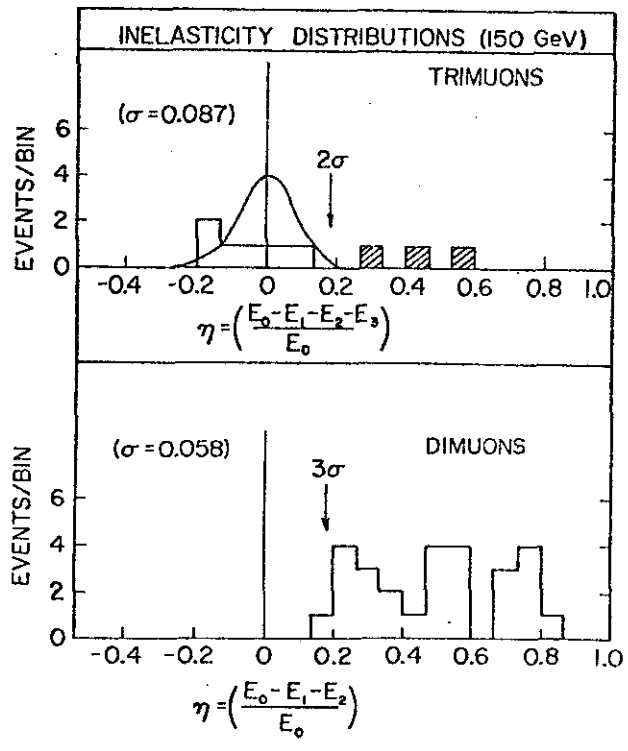

Figure 23a. Inelasticity distribution for 3μ events. Resolution on η is determined by the finite momentum resolution of the spectrometer. Note that only 3 events are outside 2σ from zero. The two ambiguous 3μ events are not plotted.

Figure 23b. Inelasticity distributions for 2μ events. Note that for all 2μ events, $\eta \geq 0.2$ corresponsing to 3σ from zero.

TABLE II

TRIMUON EVENTS

TYPE	EVENT	E_1	E_2	E_3	q^2	Y	X	W	M_{12}	M_{13}	M_{23}	Θ_{12}	Θ_{13}	Θ_{23}	ϕ_{12}	ϕ_{13}	ϕ_{23}	$(P_T)_2$	$(P_T)_3$	REMARKS
μ^-	1	-44	-31	+15	2.1	0.61	.01	14.0	1.77	1.71	0.82	48	67	38	144	166	50	0.82	0.62	$\eta > 0.2$
μ^-	2	-45	-14	+ 6	3.3	0.60	.02	13.9	2.13	1.42	0.73	136	56	84	178	163	19	0.58	0.38	$\eta > 0.2$
μ^+	3	+49	+47	-11	4.2	0.60	.02	13.6	3.17	2.33	2.36	66	100	104	144	117	99	1.66	0.89	$\eta > 0.2$
μ^+	* 4+	+65	-	-22	19.2	0.57	0.12	11.9	-	3.19	-	-	84	-	-	137	-	-	0.69	E_2 unknown
μ^+	5+	-	+19	-16	-	-	-	-	-	-	1.02	-	-	59	-	-	61	-	-	E_1 unknown
μ^-	6+	-94	-34	-	1.4	0.37	.01	10.1	2.47	-	-	43	-	-	132	-	-	.93	-	E_3 unknown
μ^-	7	-113	-51	+38	9.3	0.25	.13	7.8	3.55	1.45	0.82	47	70	59	176	106	78	2.52	0.30	$\eta < 0.2$
μ^-	8	-98	-55	+22	5.2	0.35	.05	9.7	2.99	1.63	1.77	41	35	51	177	69	114	.67	1.30	"
μ^-	9	-115	-19	+ 7	2.6	0.23	.04	8.0	2.64	2.28	1.13	57	82	101	142	107	110	.57	.51	"
μ^-	10	-138	-30	+ 8	6.0	.08	.28	4.0	3.65	1.37	0.41	57	42	27	177	139	44	4.98	1.44	"
μ^+	* 11	+39	+36	-59	3.7	.74	.02	14.3	1.77	2.70	2.44	136	56	82	178	163	133	1.02	1.68	"

* Event triggered by the leading particle.

\+ One particle traverses region of zero magnetic field

++ η is inelasticity $\left(\frac{E_0 - E_1 - E_2 - E_3}{E_0}\right)$

2. Q^2, W, x, and y distributions.

Six 3μ events do not have the same inelasticity as 2μ events. Three 3μ events (~30% of observed sample) and 2μ events have $\eta > 0.2$. The nature of the quiet events are not fully understood at this time. The same conclusion can be seen in the Q^2 vs W distribution. Figure 24 shows 85% of 2μ events are found in the region W > 8-9 GeV. Most quiet 3μ events lie outside this boundary. Thus the origin of these quiet events could conceivably be very different from the large inelasticity events.

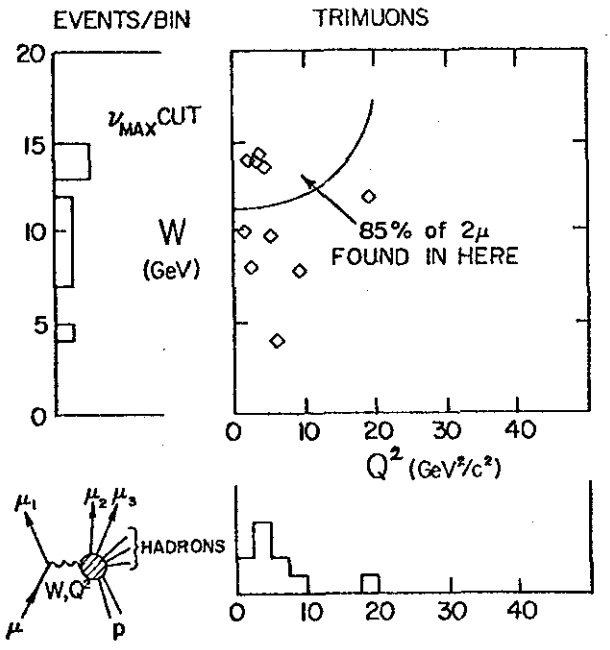

Figure 24. W vs Q^2 for 3μ events. Note that a large fraction of the 3μ events lie outside the boundary where 2μ events are found.

We show in Figure 25 and 26 x and y distributions for 3μ events. In all of these distributions we make the assumption that the leading particle is the muon having the same sign as the incoming muon and having the most energy. (See Table II)

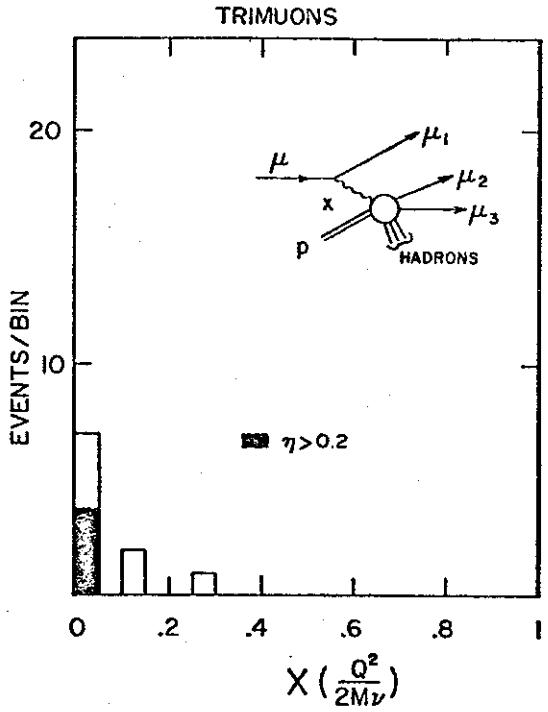

Figure 25. x distribution for 3μ events.

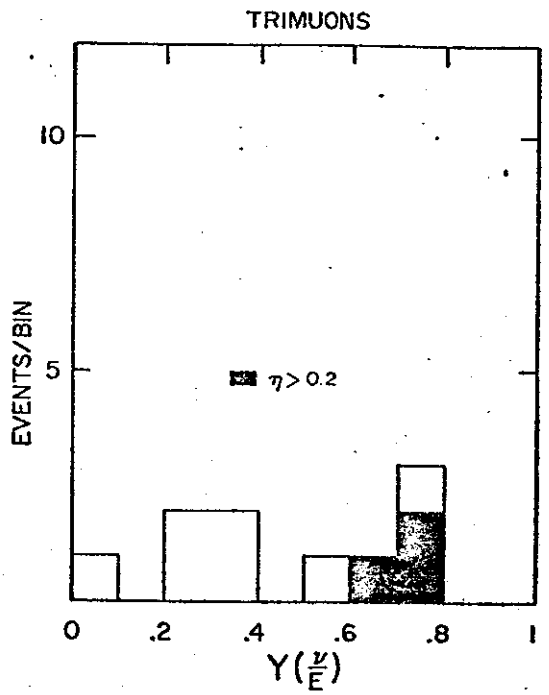

Figure 26. Y distribution for 3μ events.

3. M_{23} and M_{13} distributions.

The mass spectra for M_{13} and M_{23} [Figure 27 a) and b)] show no evidence of production of ψ or other heavy particles with masses greater than 3 GeV.

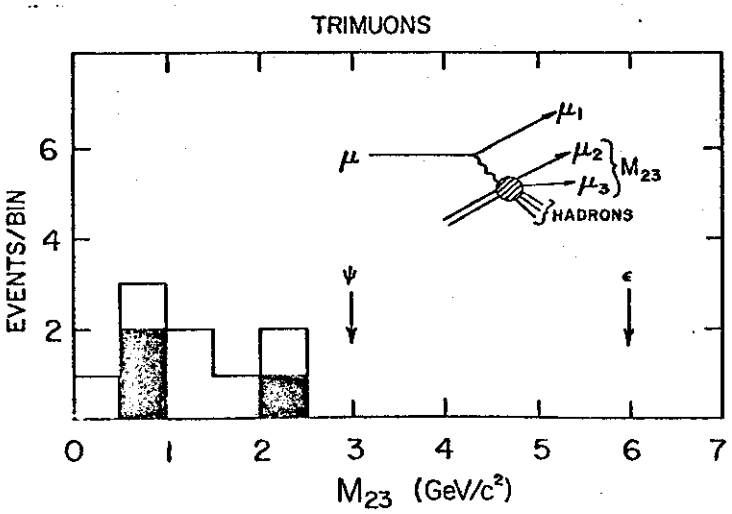

Figure 27a. Mass M_{23} distribution.

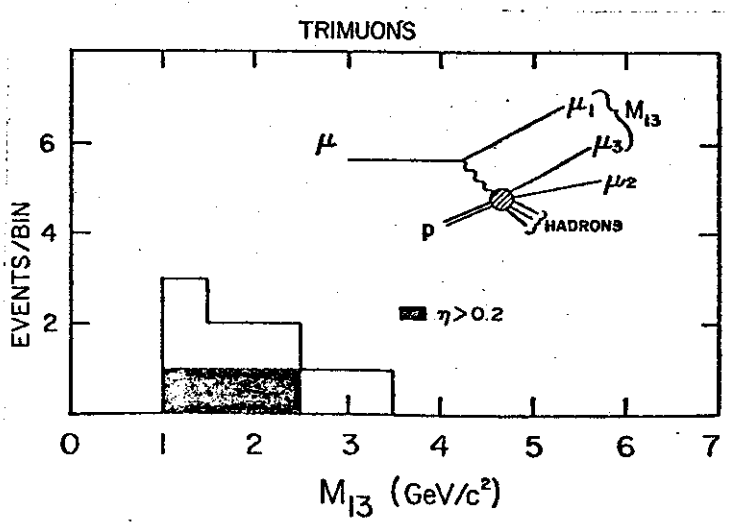

Figure 27b. Apparent mass M_{13} distribution.

5. Angular and Azimuthal Distributions of 3μ events.

The trigger for the experiment is a penetrating muon at $E_\mu > 17$ Gev and Θ_μ larger than that subtended by the trigger hodo-scopes. It is possible to accept events triggered by the non-leading muons. The probability is larger for 3μ's than 2μ's since there are two extra muons available to trigger the apparatus.

Without a production mechanism, this effect cannot be studied in detail. Experimentally, if we define the leading particle to be the more energetic like-sign muon(s) in 3μ events, we find in Figure 29 that $\theta_1(3\mu) > \theta_1(2\mu)$. This is a reflection that larger fraction of 3μ events are those triggered by the "extra" muon instead by the leading muon. There will be a larger number of leading muons to go forward at lower Q^2.

As expected, no particular correlations between Θ_2 and Θ_3 was found.(Fig. 30) In addition, $\theta_{2,3}$ distribution appears flat, as shown in Figure 29 a) and b). Fig. 31 a), b), c), and d) also show other combinations of azimuthal and production angles of the final state muons.

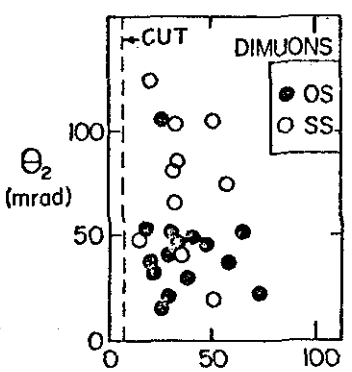

Figure 29a. Θ_2 vs $\Theta_{leading}$ for 2μ events. The lower angle cut is due to the presence of veto counters in the beam axis.

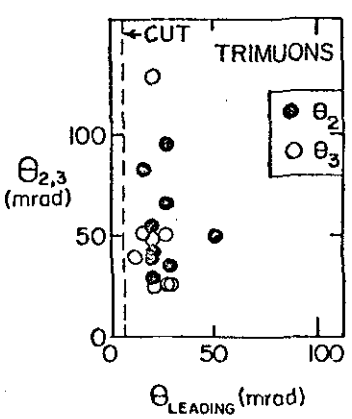

Figure 29b. $\Theta_{2,3}$ vs $\Theta_{leading}$ for 3μ's events.

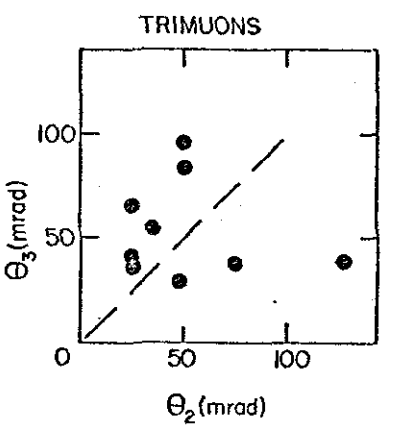

Figure 30. Θ_3 vs Θ_2 for 3μ events. No asymmetry is seen.

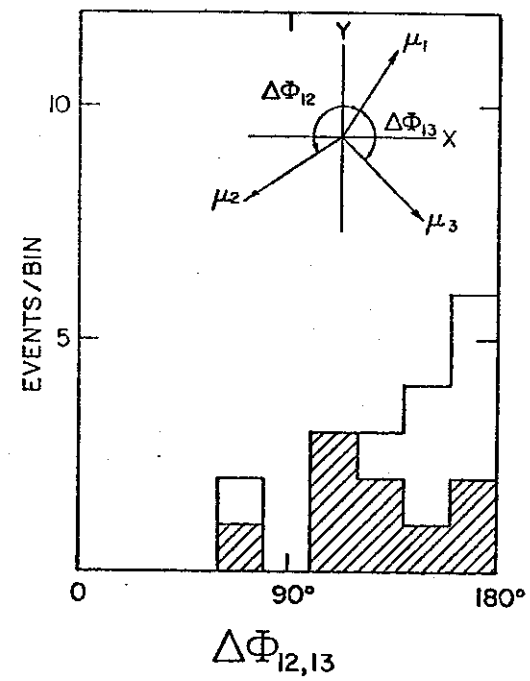

Figure 31a. $\Delta\phi_{12,13}$ for 3μ events Shaded region corresponds to $\Delta\phi_{13}$

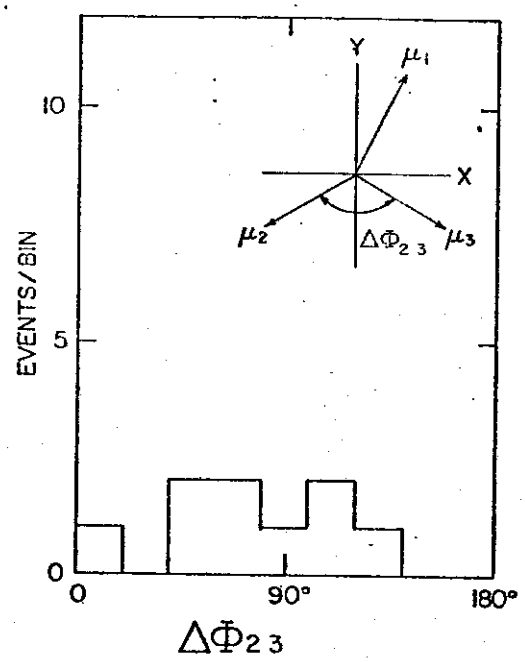

Figure 31b. $\Delta\phi_{23}$ for 3μ events.

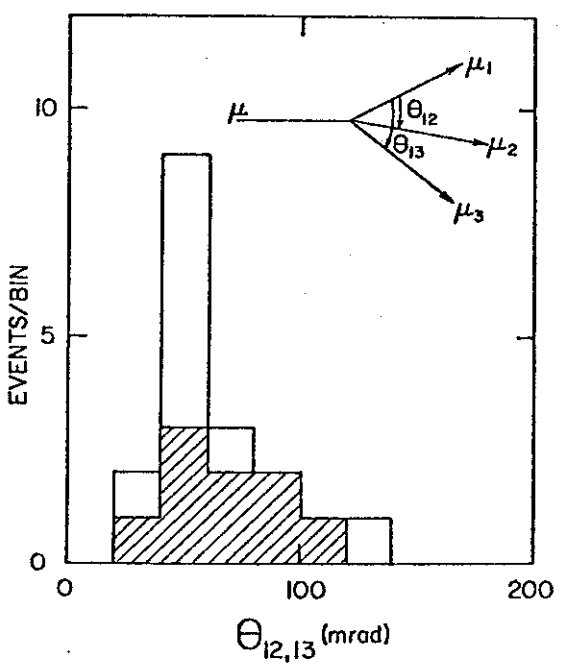

Figure 31c. $\Theta_{12,13}$ for 3μ events Shaded region corresponds to $\Delta\phi_{13}$.

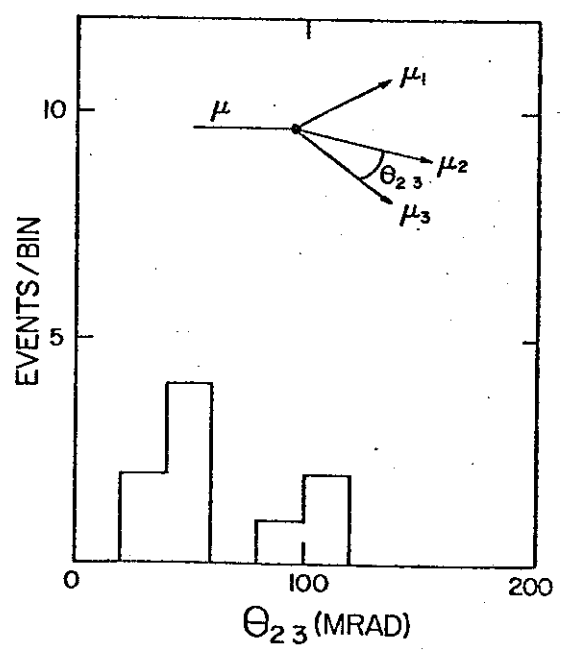

Figure 31d. Θ_{23} for 3μ events

4. $E_{2,3}$ vs $(P_T)_{2,3}$

Figure 28 shows the $E_{2,3}$ vs $(P_T)_{2,3}$ distributions, we combined the data for E_2 and E_3 as E_1 is identifiable from their more energetic penetrations. We estimate π and K backgrounds which give rise to two extra muons with $E_{2,3} > 5$ GeV to be negligible (<0.1%).

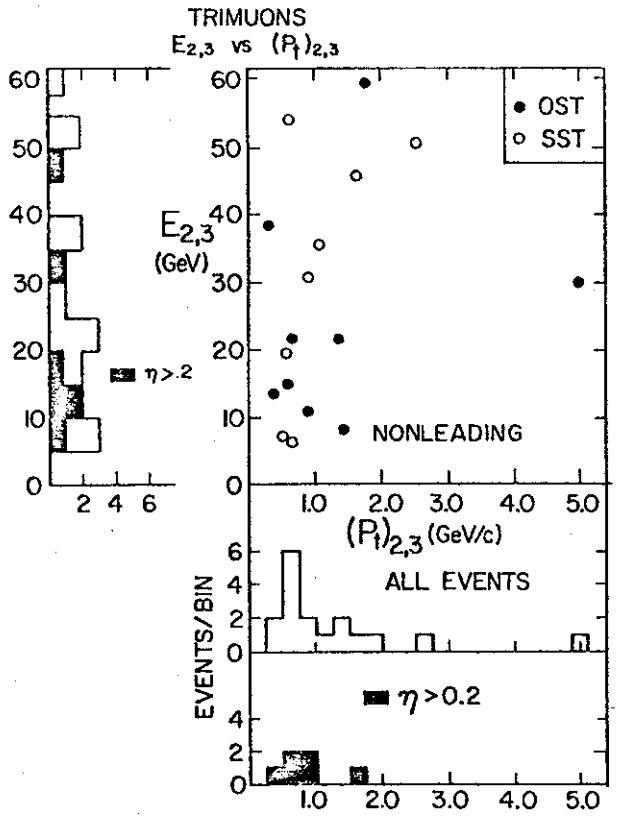

Figure 28. $E_{2,3}$ vs $(P_T)_{2,3}$ for 3μ events. OST is the muon with opposite sign to the leading muon and SST is the muon with the same sign as the leading muon. There is no observable difference between OST's and SST's.

7. Summary of Trimuon (3μ) Event Characteristics

The following characteristics are observed in the 3μ data:

1) All 3μ events show opposite signative between μ_2 and μ_3.

2) No apparent peaks in $M_{\mu\mu}$ for all opposite charge combinations M_{13}, M_{23}.

3) No events seen at ψ or ε mass.

4) There may be two classes of 3μ events:

   a) quite 3μ events, $\eta < 0.2$.

   b) inelastic events, $\eta > 0.2$.

5) Distributions in x, Y, W and Q^2 for the "inelastic" 3μ events agree reasonably well with 2μ events.

6) Distributions in x, Y, W and Q^2 for "elastic" 3μ events seem different from those of 2μ events.

7) No coplanar events have been seen between μ_2 and μ_3.

VI. Possible Mechanisms

The sources of 2μ and 3μ events in deep inelastic muon scattering could conceivably come from totally new and unsuspected physics. The statistic of 2μ events is currently at the level of dimuons observed in neutrino interactions. The 3μ events, however, have not yet been observed in either neutrino, e^+e^- or hadronic interactions either at Fermilab or ISR. The unique advantage in μ interaction is the precise knowledge of the virtual photon energy and Q^2 that lead to a multilepton final state. A large source of speculations can thus be eliminated. Another advantage is the precision with which one could determine the direction of photon. This helps enormously as it defines $(P_T)_2$ of the extra muon. Even so, the analysis of multimuon events is necessarily complex due to the inherently large number of possibilities:

I. Production of a virtual photon continuum in electro-magnetic interactions.

II. Weak decays of new resonant states including $W^{\pm}$, Z° formed by weak interaction of the incoming μ's.

III. Weak or semileptonic weak decays of hadronic states (π, K, D, $\bar{D}$, F, ...) formed by electromagnetic hadronic interaction of the virtual photon.

IV. Electromagnetic decays of resonant hadronic states (π°, η, ϕ, ω, J/ψ, ψ', ...) formed by electromagnetic or strong interaction of the virtual photon.

V. Production and decay of heavy leptons in electromagnetic interactions.

It is much too early to pin point exactly the nature of the production mechanism due to the limited statistics. A few obvious cases can be easily ruled out at this time from the observed characteristics of multimuon events. Table III shows average quantities of the 3μ, 2μ, and 1μ event.

1. Heavy Leptons

Heavy leptons can be produced in μ collision through a Bethe-Heitler mechanism.[13] It is unlikely that the 2μ sample could be due to the production of heavy leptons in the same sense that QED trident cannot fake 2μ events easily. However, for the quiet 3μ events, these possibilities cannot be ruled out. Trimuon events tend to have "larger" P_T than those expected from QED tridents. No firm conclusion can be drawn from the available data or calculations on heavy lepton production. Further studies along this line are continuing.

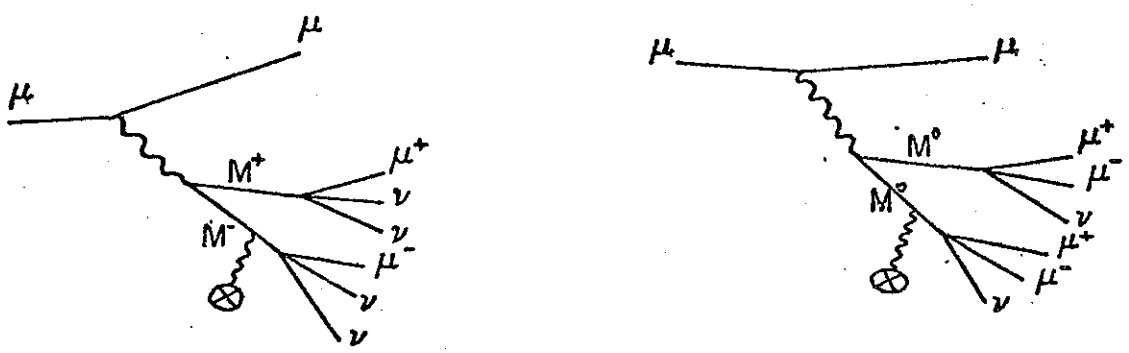

Figure 32. Mechanisms for $M^{\pm}$, M^{0} production in muon interactions

Neutral heavy lepton $\overline{M}^\circ$ of the gauge theory variety is not favored in our data since the production occurs at the leading muon vertex. This necessarily contradicts the observed x, W and Y distributions. Also, cross section calculations for $\overline{M}^\circ$ production ($\mu p \rightarrow \mu + \overline{M}^\circ + X$; $\overline{M}^\circ \rightarrow \mu^+\mu^-$) tends to be low ($\sigma \sim 2 \times 10^{-37}$ cm^2 at $\overline{M}^\circ$ = 5 GeV) to account for all of the 2μ sample.[14] In the future it would be of interest to examine what considerations similar to Pais-Treiman relation[15] can be applied to muon interactions.

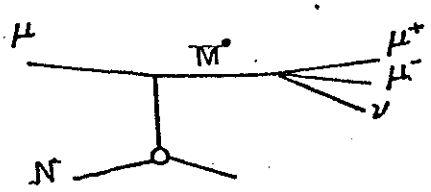

Figure 33. $\overline{M}^\circ$ production at the muon vertex

TABLE III

AVERAGE QUANTITIES FOR DEEP INELASTIC, DIMUONS AND TRIMUON EVENTS

TYPE	$\langle E_1 \rangle$ (LEADING)	$\langle E_2 \rangle$	$\langle E_3 \rangle$	$\langle x \rangle$	$\langle Q^2 \rangle$	$\langle W \rangle$	$\langle \nu \rangle$	$(P_T)_2$	$(P_T)_3$	NO. OF EVENTS
1μ	55.0	Not Applicable	N.A.	0.11	15.0	12.5	0.64	N.A.	N.A.	25560
2μ	55.4	20	N.A.	0.048	7.5	13.0	0.65	0.88	N.A.	27
3μ[a]	45.0	30	11	0.02	3.2	13.8	0.60	1.02	0.60	3
3μ[b]	100.0	34	25	0.09	4.7	9.0	0.34	1.77	1.04	6

a Inelasticity $\eta > 0.2$ only

b $\eta < 0.2$ events

2. Weak Bosons

The weak decay of resonant states $W^{\pm}$, Z°, B°, etc., formed in a weak process are unlikely mechanisms[16] for the observed 2μ and 3μ events. Characteristics of our data do not favor these possibilities. We also note that recent theoretical development of unified theories of the weak and electromagnetic interactions also suggest masses of $M_{W^{\pm}}$, $M_{Z^{\circ}}$ = order of 100 GeV/c^2, a sensitivity no current experiments at Fermilab can hope to achieve.

Characteristics of $W^{\pm}$, Z°. ... productions are:

1. Process should be elastic
2. $(P_T)_2$ should be large up to $P_T \sim (\frac{M_W}{2})$
3. Cross section $\sim 10^{-39}$ cm^2.
4. Should show no leading particle effect.

These characteristics are not found in the data.

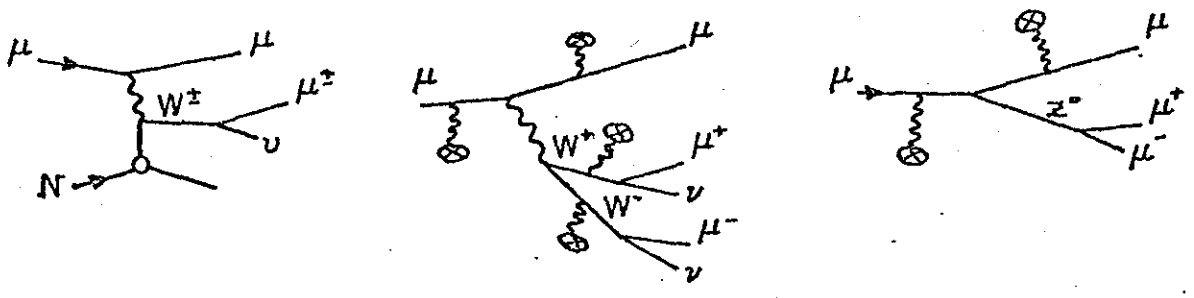

Figure 34. Production of weak bonsons $W^{\pm}$, Z^{0} in muon interactions.

3. Electromagnetic Mechanisms (QED)

One would expect electromagnetic process to have some role in the production of leptons in virtual photon interactions with matter. The most prominent processes are coherent or incoherent production of electromagnetic tridents.[12] Fortunately, the detection apparatus has a built-in suppression against these processes which occurs mostly at low 4-momentum transfers of the virtual photon or muon propagators. Figure

35 shows possible processes in trident production. As we discussed previously, to be observed as 2μ events, one of the trident muons must escape detection either due to a low energy cut-off or geometrical inefficiencies. This occurs at a low probability. For 3μ events, the geometric detection of all 3μ's is good, although kinematic suppression is enormous. The coherent production goes as

$$d\sigma \sim \frac{Z^2 \alpha^4}{t^2 m_\gamma^4 \, (M^{*2} - M_\mu^2)^2} \qquad (1)$$

Only tridents with all propagators near M_μ^2 are produced with appreciable cross section. Our apparatus has exceedingly small acceptances for propagator masses < 1 GeV. The suppression is $\sim 10^6$-10^8 from the total cross section of 1 μb in an iron nucleus.

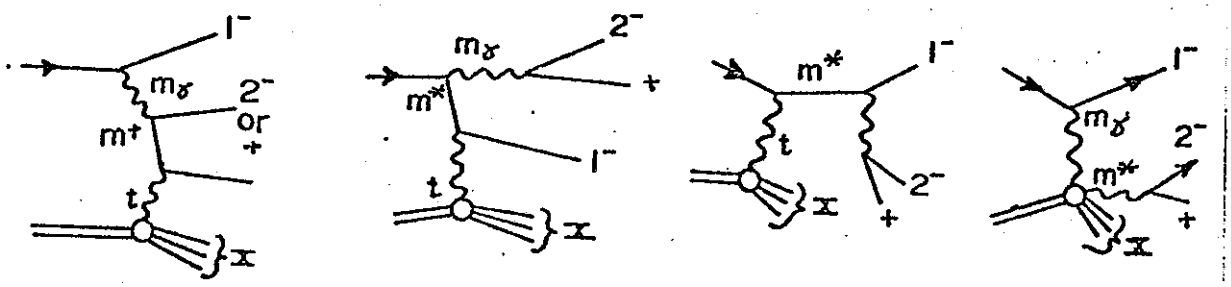

Figure 35. Bethe-Heilter, bremsstrahlung and deep compton trident production processes.

Characteristics of QED tridents are:

1) Most coherent processes (except incoherent tridents)

2) Small relative opening angles between produced muons

3) Small P_T relative to virtual photons

4) Cross section peaks at low masses ($\sim m_\mu$)

5) Calculated σ ranges from 10^{-36}cm^2 for coherent processes to 10^{-38}cm^2 for incoherent processes for events with propagators > 1 GeV^2.

We have yet to do a rigorous (and tedious) calculation of these processes which take into consideration apparatus acceptances. Preliminary estimates (good to an order of magnitude) yield a background level of ≈ 0.04 events for coherent 3μ events and 0.4 events for incoherent 3μ events. These processes cannot be expected to account for all the extra muon events.

4. Vector Meson Production

A large class of vector mesons, ρ, ω, η, ψ, . . . can be produced in deep inelastic muon scattering. If these vector mesons are allowed to decay

electromagnetically in two muons, trimuons can result. In addition, if one of the decay muons should escape detection, a simulated 2μ events will result.

The characteristics of these events will be

1) Generally μ_2 or μ_3 has low P_T (< 0.5 GeV/c)

2) Azimuthal angles between μ_2 and μ_3 should be $\sim 180^0$.

3) Mass peak at ρ, ω, and ϕ.

Various features observed in the data do not agree well with these characteristics. P_T for nearly all observed 2μ or 3μ events is $\geq$ 0.5 GeV/c,

Some of the possible background processes considered are listed:

$$\begin{aligned}
&\mu N \to \mu\rho X; \quad \rho \to \mu^+\mu^- \\
&\mu N \to \mu\rho X; \quad \rho \to \pi^+\pi^- \to \mu^+\mu^- \\
&\mu N \to \mu\eta X; \quad \eta \to \gamma\mu^+\mu^- \\
&\mu N \to \mu\phi X; \quad \phi \to K^+K^- \to \mu^+\mu^- \\
&\mu N \to \mu K_S^o X; \quad K_S^o \to \pi^+\pi^- \to \mu^+\mu^- \\
&\mu N \to \mu K_L^o X; \quad K_L^o \to \pi\mu\nu \to \mu^+\mu^-
\end{aligned} \tag{2}$$

Contamination due to these processes are found to be negligible.

5. <u>Semileptonic Weak Decay of New Hadrons</u>

This class of mechanisms is viable if produced resonant states are stable under the strong and electromagnetic interactions. Otherwise, the (semi-) leptonic branching ratios will be small.

We have shown that π/K background should contribute to less than 20% of all 2μ events, and even less so for 3μ events. We shall focus our attention to the remaining direct (unknown) sources of lepton yields.

Current interest is focussed on the possibility that there are significant associated production of the new hadrons M_C (either pseudoscalars, D, or F, and the vector mesons D* or F*), which are predicted by the 4-quark model. Presumably the leptons could come from the semileptonic decays of $M_C \to x + \ell + \bar{\nu}$. Associated production of $M_C\bar{M}_C$ could then give rise to both 2μ and 3μ final states with the rate governed by the decay

branching ratio. The process will proceed as follows:

$$\begin{array}{l} \mu N \to \mu + M_c + \overline{M}_c + X \\ \qquad\qquad\quad \hookrightarrow \mu + \nu + X \\ \qquad\qquad \hookrightarrow \mu + \nu + X \end{array} \tag{3}$$

We do not yet know the precise production mechanism. It is difficult to extract the branching ratio from the data since the acceptances depend on the masses, angular distributions and energy spectra of the produced hadrons. However, most features observed in the dimuon data tend to agree well with those expected in semileptonic weak decays of M_c.

1. Small x enhancement $\langle x \rangle_{2\mu} = 0.048$
2. Apparent threshold in $W \sim 8$-9 GeV
3. High visible hadron inelasticity $\eta > 0.2$ (30 GeV).
4. Flattish $(P_T)_2$ distribution ($\frac{dn}{dp_T} \sim e^{-1.8P_T}$) , $P_2 > 0.5$ GeV/c.
5. No events found at very large $(P_T)_2 > 2.5$ GeV/c.

We made an attempt to simulate the production and decay of new hadrons. Our model assumes the associated production of $D\overline{D}$ with $M_c = 2$ GeV. The new hadron is produced as[4]

$$\frac{d\sigma}{dyd^2p_T} = 0.6\ \mu b/(GeV)^2 \quad \exp\ (-2p_T/(GeV/c)) \tag{4}$$

decaying isotropically via $M_c \to K + \mu + \nu$ having a branching ratio of 10-30%. Shapes of the P_T and P_2 distributions are in good agreement with observed distributions except for the low normalization of the spectra. We conclude that unless more than one type of new hadrons are being produced the normalization remains an anomally. We are currently making attempts to use other fits.

VII. Branching Ratios

1. $\sigma(\mu \to \mu\mu)/\sigma(\mu \to \mu)$

From Table I we see that in 12 dimuon events (out of 27) the leading muon had the same trigger requirement as deep inelastic events. Assuming <20% π/K backgrounds, $\lesssim$ 20% loss due to scanning or veto counters and (0.5 ± 0.25) for the detection of the extra muon, we obtain a branching ratio.

$$B_{2\mu} = \frac{\sigma(\mu \to \mu\mu)}{\sigma(\mu \to \mu)} = (1.0 \pm 0.5) \times 10^{-3} \tag{5}$$

2. $\sigma(\mu \to \mu\mu\mu)/\sigma(\mu \to \mu\mu)$

This number is a very important one since it may represent the direct measurement of semileptonic weak decay branching ratio of new hadrons, if these particles are indeed associated-produced in μN collisions. However this number is also very difficult to determine correctly since the detection efficiencies for μ_2 and μ_3 must both be understood.

The best way is to insist that events to be used in branching ratio calculations must have the same triggering criteria: leading particle μ_1 triggers the apparatus. This eliminates completely the need to know the acceptance for μ_1. Unfortunately, most of the multimuon events found do not contain μ_1 that triggered the apparatus. In fact for 3μ events, either μ_2 or μ_3 did the triggering. For 2μ events, 12 μ_1 triggered the apparatus out of 27 accepted events. If one takes into consideration of the detections efficiencies we have

$$\frac{\text{No. of } 3\mu \text{ events}}{\text{No. of } 2\mu \text{ events}} \doteq \frac{\sigma B^2}{\sigma\{2B(1-B)\}} \tag{6}$$

where B denotes the semileptonic weak decay branching of M_c. At 90% confidence level, we found $B < 0.3$. When statistics improves, a good number can be expected.

One may want to examine the three 3μ events with inelasticity $\eta > 0.2$. These events can be compared with 27 dimuons with $\eta > 0.2$. Although the uncorrected ratio is about 0.1, we need more analysis to get a more reliable number since a production mechnanism and decay scheme must be assumed to make the detection efficiency corrections.

Finally if we assume that $B \lesssim 0.3$ and that M_c is produced in μN scattering, then combining (5) and (6),

$$\frac{\sigma(\mu \to \mu c\bar{c})}{\sigma(\mu \to \mu)} \gtrsim 3 \times 10^{-3} \tag{7}$$

VIII. Conclusions

It is our conjecture that new particles are produced in deep inelastic muon collisions. This conjecture is strengthened by the following further considerations:

i) The events at large Q^2 ($> 2\ \text{GeV}^2/c^2$) distinguishing themselves from the "soft" processes that prevail in conventional hadronic and electromagnetic interactions: heavy objects can not be easily processed by such processes.

ii) Virtual or real photons can produce particles that are not already present as target constituents. A good example is the photoproduction of ψ/J at SLAC, Cornell and Fermilab.[17]

iii) A direct comparison of the absolute yields in single muon deep inelastic scattering[2] from those expected from the SLAC data show a 15% excess of events at large values of $\omega(\omega > 10)$. (Figure 4). This is the same ω region where our extra muons are found.

Combining our current experimental observation and our published results on deviation from scaling, we infer that high W (or ν)events may be due to our exciting new degrees of hadronic freedome in deep inelastic collisions. If the mass of the new hadron is m_c, the threshold for excitation occurs at $W^2_{th} = (2m_c m_N)^2$ and $q^2_{th} = n\, m_c^2$, where n is a model dependent quantity of order 1. Near the q^2-threshold the new hadron production cross-section should be nearly flat, where conventional vector meson production cross-section is already dropping rapidly. Naturally one expects to have an enrichment of the order of $(\frac{m_c}{m_\rho})^2 \simeq 10$.

IX. Current and future plans

Further data are clearly needed. In the near future, the Michigan State-Fermilab muon experiment can soon provide:

1. A large data sample ($\geq$ 1000 2μ, 100 3μ events)
2. Determination of the missing energy, $E_m = E_0 - E_1 - E_2 - E_3 - E_h$
3. Mass spectra in muoproduction.
4. More precise measurements of branching ratios.
5. Visible hadron energy distributions.

Data daking commences in July, 1976. Following this experiment, another experiment (Berkeley-Princeton-Fermilab) will do similar measurements.

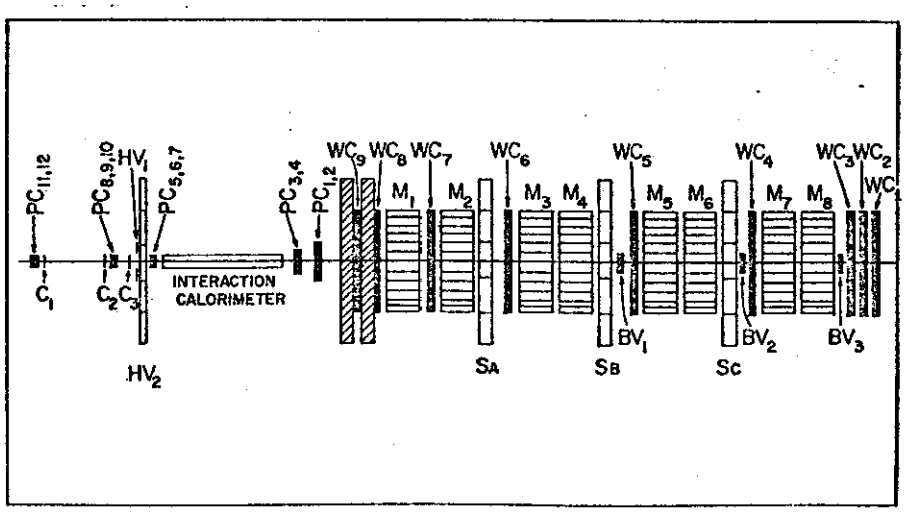

Fig. 36 Michigan State-Fermilab muon experiment now in progress at Fermilab. The interaction calorimeter is 24 feet in length compared to 6 feet in the experiment discussed here.

X Acknowledgements

I wish to acknowledge contributions made by various members of the Cornell-Michigan State-UCB-UCSD collaboration during the data-collection phase and during analysis to test scaling. The multimuon events presented here were found in the data sample of E-26. C. Chang and J. Hoekzema made substantial contributions to event-finding and A. VanGinneken wrote an excellent background Monte-Carlo.

Discussions with M. Einhorn, C. Albright, L. Litt, and M. Tannebaum were fruitful. Finally I acknowledge an article sent by A. DeRújula suggesting that multimuon events ought be seen in deep inelastic muon interactions.

REFERENCES

1. Y. Watanabe et. al, Phys. Rev. Lett. 35, 898 (1975)
2. C. Chang et. al, Phys. Rev. Lett. 35, 901 (1975)
3. S. D. Drell and T. M. Yan, Annals of Physics, 66, 518 (1971)
4. See Review Articles by L. Lederman, Proceedings of the International Conference on Lepton and Photon Interactions at High Energies, Stanford, California, 1975; J. D. Sillivan, Proceedings of Conference on New Results in High Energy Physics, Vanderbilt University, 1976
5. B. Aubert et. al.. Phys. Rev. Lett. 33,984 (1974)
6. J. J. Aubert et. al., Phys. Rev. Lett. 33, 1404 (1974)
7. J. E. Augustin et. al., Phys. Rev. Lett. 33, 1406 (1974) and 1453 (1974)
8. A. Benvenuti et. al., Phys. Rev. Lett. 34, 419 (1975)
9. K. W. Chen, Proceedings of International Conference on High Energy Physics, Palermo, Italy, 1975
10. C. Chang, Ph.D. Thesis, MSU-CSL-31, 1976 (unpublished)
11. W. A. Loomis, et. al., Phys. Rev. Lett. 35, 1483 (1975)
12. S. Brodsky and S. Ting, Phys. Rev. 145, 1018 (1966)
13. Y. S. Tsai, Rev. Mod. Phys. 46, No. 4
14. R. W. Brown et. al., Phys. Rev.
15. A. Pais and S. B. Treiman, Phys. Rev. Lett. 35, 1206 (1975)
16. J. Smith, et. al., Phys. Rev. D5, 158 (1972); ibid p. 177.
17. See for example, Knapp et. al., Phys. Rev. Lett. 34, 1044 (1975).